The Limb-Correction of ATMS Brightness Temperature and its Applications to Analyzing Tropical Cyclone Intensity Changes

Tyler Wawrzyniak

A scholarly paper in fulfillment of the requirements for a degree of

Master of Science

May 2020

Department of Atmospheric and Oceanic Science

University of Maryland

College Park, Maryland

Advisor: Dr. Da-Lin Zhang

Table of Contents

Abstract

The ATMS instrument on the Suomi-NPP and NOAA-20 polar-orbiting satellites measures radiation from the Earth's atmosphere and surface. The instrument has 96 horizontal beam positions, causing the satellite signal to travel a longer distance in the atmosphere for the locations that are off of nadir. Consequently, the image of brightness temperatures is skewed and prevents the direct visualization of important weather features. Therefore, this work, applies a limb-correction algorithm (*Zhang et al.*, 2017) to resolve the issue. The algorithm mitigates the difference introduced by varying optical paths of the satellite signal for each beam position. Limb-corrected ATMS data are used to study time evolution of the upper-level warm core of tropical cyclones. Surface pressure tendency of multiple hurricanes was hydrostatically estimated using retrieved temperature profiles, with separate coefficients for clear and cloudy sky conditions. The technique's validity was tested on Hurricanes Florence (2018), Michael (2018), and Dorian (2019). Results show the surface pressure tendency so obtained compares reasonably well to the best track surface pressure tendency in all three cases. Though surface pressure was not exactly equal to the best track surface pressure, the calculated surface pressure tendency from the ATMS data was able to follow the best track pressure trends due to the dominant influences of the upper-level warm core during the hurricanes' lifetimes. However, near the edge of the satellite scan the retrieved temperature was unable to accurately resolve the upper-level warm core due to large errors in the temperature retrieved from the ATMS brightness temperature and the degraded spatial resolution at the edge of ATMS scan. Away from these regions, the surface pressure tendency algorithm was able to more reasonably match the best track pressure tendency. Future work would involve refining the temperature retrieval and estimating wind speed tendency using the gradient wind balance equation and surface pressure tendency calculated from the ATMS data.

Acknowledgements

I would like to thank my advisor, Da-Lin Zhang, for guiding me during the research process while conducting my graduate studies. Also, I would like to thank NESDIS for funding my research and providing me with instruction and experience with satellite-based research. In particular, I would like to thank Lihang Zhou and Quanhua (Mark) Liu for their assistance and guidance. They introduced me to the methods used to conduct research in a useful and meaningful way that creates a beneficial product. Additionally, thank you to NOAA's Comprehensive Large Array-data Stewardship System (CLASS) for providing easy online access to download ATMS data files for my research. Lastly, I would like to thank Tammy Hendershot, the Department of Atmospheric and Oceanic Sciences program coordinator, for all of her assistance and guidance in my pursuit of a master's degree. This project was supported by NESDIS through a grant provided by CISESS.

List of Tables

List of Figures

Chapter 1 Introduction

1.1 ATMS Brightness Temperature

The Advanced Technology Microwave Sounder (ATMS) is carried on the Suomi National Polar-orbiting Partnership (Suomi-NPP) and NOAA-20 satellites. The ATMS instrument is a combination of the temperature and moisture sounding capabilities of the Advanced Microwave Sounding Unit-A (AMSU-A) and the microwave humidity sounder Advanced Microwave Sounding Unit-B (AMSU-B), with a higher spatial resolution and calibration accuracy (*Goldberg et al.,* 2013; *Zhang et al.,* 2017).

ATMS contains 22 microwave channels between 23 GHz and 183 GHz to allow for temperature and moisture retrievals in all weather conditions. The characteristics of the ATMS instrument housed on both the Suomi-NPP and NOAA-20 satellites is shown in **Table 1**. Channels 1 and 2 are window channels that are used to provide water vapor, cloud water, and surface emissivity data required to retrieve accurate temperature profiles (*Goldberg et al.,* 2013*; Zhang et al.,* 2017). These channels are especially important in determining regions of clear and cloudy sky conditions. Channels 3 – 15 provide information necessary for vertical temperature profiles from the surface up to 3 hPa (~37km altitude). Moisture profile information is retrieved from channels 18 – 22, which are similar to the humidity sounder profiles observed by the AMSU-B sounder and Microwave Humidity Sounder (MHS). The instrument scans horizontally ±52.725° from nadir at each side, with 96 fields of view separated by 1.11° that have a total scan swath of 2700 km (*Yan et al.,* 2020).

***Table 1**: Suomi-NPP Advanced Technology Microwave Sounder (ATMS) characteristics (Weng et al., 2013).*

Channel	Center Frequency (GHz)	Polarization	FOV (°)	Weighting Function Peaks
1	23.8	V	5.2	Window (Surface)
2	31.4	V	5.2	Window (Surface)
3	50.3	H	2.2	Window (Surface)
4	51.76	H	2.2	Window (Surface)
5	52.8	H	2.2	Low sounding
6	53.596 ± 0.115	H	2.2	4 km – 700 hPa
7	54.40	H	2.2	9 km – 400 hPa
8	54.94	H	2.2	11 km – 250 hPa
9	55.50	H	2.2	13 km – 180 hPa
10	57.2903	H	2.2	17 km – 90 hPa
11	57.2903 ± 0.115	H	2.2	19 km – 50 hPa
12	57.2903	H	2.2	25 km- 25 hPa
13	57.2903 ± 0.322	H	2.2	29 km – 10 hPa
14	57.2903 ± 0.322 ± 0.010	H	2.2	32 km – 6 hPa
15	57.2903 ± 0.322 ± 0.004	H	2.2	37 km – 3 hPa
16	87 – 91 (88.20)	V	2.2	Window (Surface)
17	165.5	H	1.1	H_2O 18 mm
18	183.31 ± 7	H	1.1	H_2O 18 mm
19	183.31 ± 4.5	H	1.1	H_2O 4.5 mm
20	183.31 ± 3	H	1.1	H_2O 2.5 mm
21	183.31 ± 1.8	H	1.1	H_2O 1.2 mm
22	183.31 ± 1.0	H	1.1	H_2O 0.5 mm

Figure 1 displays the ATMS weighting function of the U.S. standard atmosphere provided by the Community Radiative Transfer Model (CRTM) over a water surface for all 22 channels. The left figure shows channels 1 – 15, which are all of the channels associated with vertical

temperature retrievals in the atmosphere. The weighting functions in the figure on the right represent the moisture information retrieved through channels 16 – 22 of the ATMS instrument.

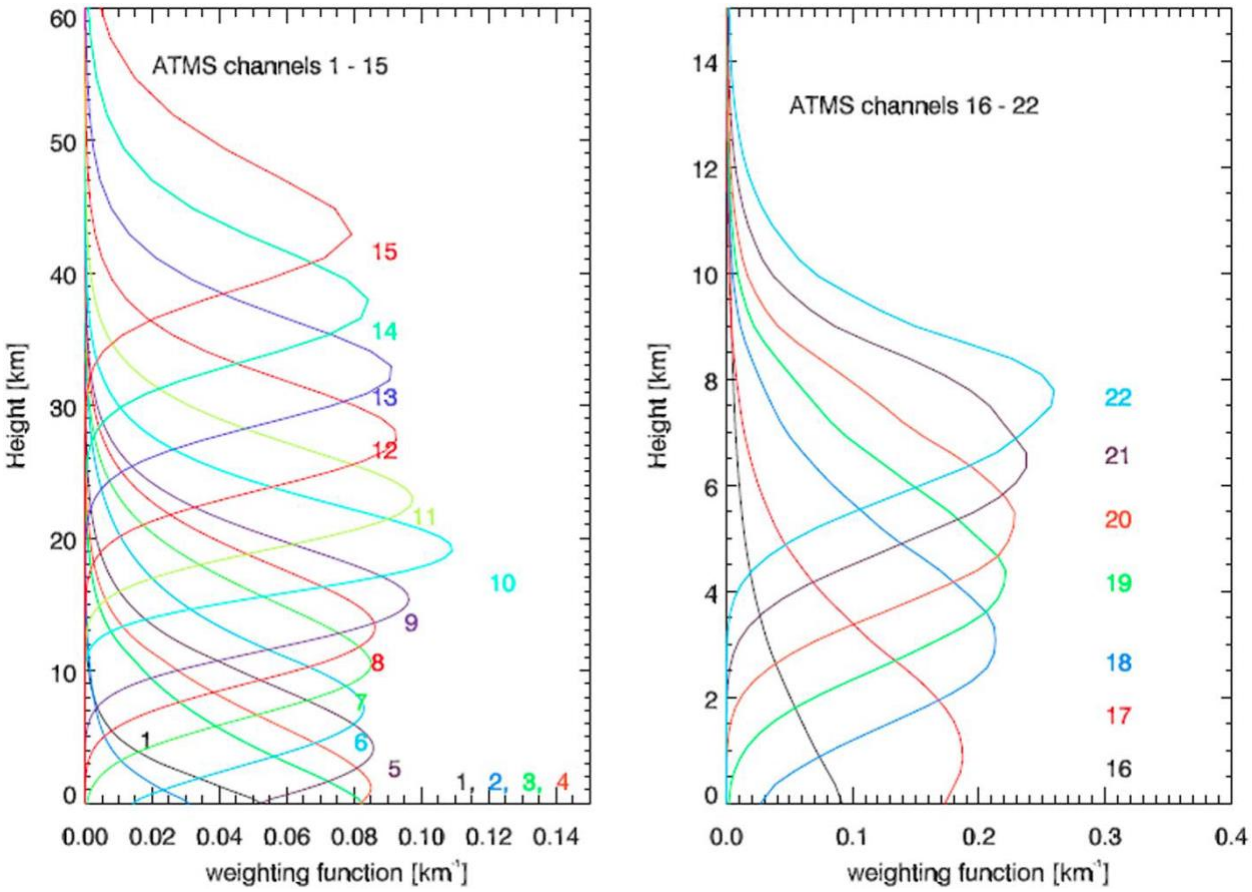

Figure 1*: ATMS weighting function of the U.S. standard atmosphere over a water surface based on the Community Radiative Transfer Model (CRTM) (Zhang et al., 2017).*

1.2 Limb-Correction Algorithm

As the instrument scans horizontally, the microwave signal has a different optical path for each beam position. The optical path is much shorter when the ATMS instrument is looking straight below the satellite at nadir when compared to extreme horizontal scan positions. Longer optical paths at the edge of the instrument scan cause the peak of the channel's weighting function to shift to higher altitudes in the atmosphere. This can result in brightness temperature difference

as high as 30 K for window channels at extreme scan positions farthest away from nadir (*Zhang et al.,* 2017). To account for this difference at the edge of the scan, a limb-correction algorithm developed by NOAA (*Goldberg et al.,* 2001*; Zhang et al.,* 2017) has been implemented. This algorithm consists of a linear combination of associated channels to account for the limb bias in the retrieval of brightness temperature for the ATMS instrument (*Zhu et al*., 2002). The associated channels were chosen based on the channel of interest as well as channels whose weighting function peaked at altitudes above and below the channels of interest that were statistically correlated (*Zhang et al.*, 2017). A set of coefficients was generated over both land and water using a training dataset to incorporate into the limb-correction algorithm. Two sets of coefficients were required because of the different radiative properties for land and water surfaces.

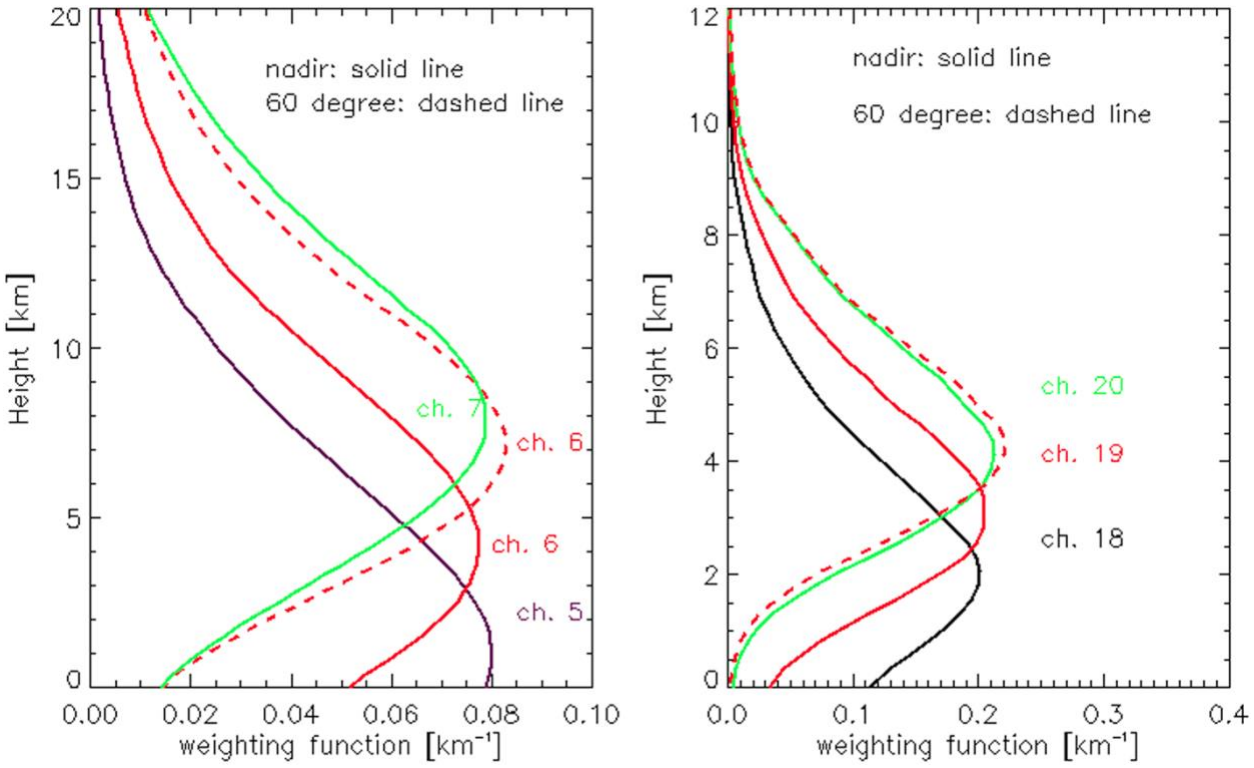

Figure 2*: ATMS channels 6 and 19 weighting function of U.S. standard atmosphere over a water surface based on the CRTM that get shifted up for measurements taken from nadir (solid)*

those taken at 60 degrees (dashed). Channels 5, 7, 18, and 20 are plotted to compare the altitude of peaking heights for these channels (Zhang et al., 2017).

The limb effect is clearly represented in **Figure 2**. In the plot on the left, the peaks of the weighting functions for locations at nadir for the instrument scan are displayed as solid lines for ATMS channels 5, 6, and 7. The dashed lines show the weighting function curve for ATMS channel 6 for locations measured at 60 degrees off nadir. Measurements taken at large angles off nadir cause the weighting functions to shift up in altitude, which is the case here with channel 6. In fact, the peak of the weighting function for channel 6 at 60 degrees off nadir is at nearly the same altitude as the peak of the weighting function for channel 7 at nadir. It is clear that off nadir measurements experience large biases when compared to measurements taken at nadir.

1.3 Tropical Cyclone Upper-Level Warm Core

The center of hurricanes are usually several degrees warmer than the surrounding environment, making them warm-core cyclones. This is in contrast to many cyclones in the mid-latitudes, which have cold anomalies in the center and are often labeled cold-core cyclones. Warm cores develop in the center of tropical cyclones due to subsidence warming of sinking air in the eye and latent heat release from intense convection (*Zhang and Chen,* 2012), particularly in the eyewall (*Zou et al.,* 2018). Upper-tropospheric warm cores are strengthened by subsidence induced by convective bursts during the onset of rapid intensification of tropical cyclones. Therefore, it has been shown there is a correlation between the intensity of the warm core anomaly and the strength of the associated hurricane (*Zhang and Chen,* 2012; *Zou et al.,* 2018; *Durden,* 2013). The height of the warm core of a hurricane is variable depending on the storm. *Zhang and Chen* (2012) showed that the warm core of Hurricane Wilma (2005) is peaked between 12 – 16 km (~300 – 125 hPa) above the surface.

Satellite data provides the opportunity to observe hurricane warm core development over remote oceans where in-situ measurements are scarce (*Zhu et al*., 2002; *Tian et al.*, 2016*; Zou et al.*, 2018; *Han and Weng*, 2018). The ATMS instrument on Suomi-NPP and NOAA-20 satellites is able to retrieve warm core anomalies throughout the duration of the event no matter how remote the storm is. However, precipitation within the atmospheric column can lead to incorrect brightness temperature retrievals. This is due to microwave contamination caused by large precipitation droplets (*Tian and Zou*, 2016; *Zhang et al.*, 2018; *Han et al.*, 2019). As a result, an anomalous cold pool is observed in the low levels of the center of a hurricane where a warm anomaly should be instead. This requires the development of different retrieval process for cloudy and clear sky conditions to mitigate the effects of the precipitation contamination of the microwave radiation (*Yan et al.*, 2020; *Han and Weng*, 2018).

The rest of this scholarly paper is organized as follows. The next chapter details the data used for this paper. Chapter 3 describes the methodology taken to investigate tropical cyclones using limb-corrected ATMS brightness temperature. Next, the results of the analysis are presented, focusing on Hurricane Dorian (2019), Florence (2018), and Michael (2018). These results look at the time evolution of the upper-level warm core and its hydrostatic relationship with surface pressure tendency. The final section of this paper summarizes the results and presents the conclusions and closing thoughts on the outcome of this study.

Chapter 2 Data

2.1 Observations

2.1.1 ATMS Brightness Temperature

The ATMS instrument on the Suomi-NPP and NOAA-20 satellites collects brightness temperatures for the profiles of the atmospheric temperatures and moistures. Brightness temperature is defined as the temperature of a black body in thermal equilibrium with its surrounding environment. An algorithm is applied to the antenna temperatures in the ATMS Temperature Data Record (TDR) dataset to calculate the brightness temperature. Geolocation, time, instrument, and other satellite data are also recorded by the ATMS instrument for visualization and analysis purposes. The brightness temperatures are contained in a 3D array that has 180 rows along the orbital direction, 96 columns to represent the scan positions, and 22 channels to represent microwave peaking heights.

2.1.2 Tropical Cyclone Best Track Data

Tropical cyclone data are collected for the National Hurricane Center (NHC) using dropsondes deployed in hurricanes by Hurricane Hunter aircraft. These dropsondes record vital information about the storm, such as surface pressure and wind speed. This information was retrieved from the National Hurricane Center's advisory archive website (https://www.nhc.noaa.gov/data/) to use as a comparison with the retrieved surface pressure from ATMS brightness temperature. This website makes all advisory data from previous Atlantic hurricanes publicly available for reference in case studies.

Additionally, Hurricanes Florence and Michael of 2018 have had tropical storm reports published by the National Hurricane Center (*Beven II et al.*, 2019; *Stewart et al.*, 2018). These reports provide detailed descriptions of the hurricanes' meteorological history and list updated and

corrected information about wind intensity, surface pressure, and storm location from the advisory data. These reports are used as a reference for comparing the retrieved results to be described in the next chapter. However, since Hurricane Dorian occurred in 2019, a tropical cyclone report has not been published for this storm at the time this document is being written. Therefore, the analysis on Dorian in the later sections was based solely on observations provided by the advisory data.

2.2 Model Data

2.2.1 ECMWF Forecast Data

To calculate the coefficients required to convert ATMS brightness temperatures to vertical temperature soundings, model data was needed to fit the satellite observations to the expected temperature. *Yan et al.* (2020) chose the European Centre for Medium-Range Weather Forecasts (ECMWF) daily forecast output as the temperature to fit ATMS data using multiple linear regression analysis. Collocated ECMWF data with ATMS brightness temperature were used to calculate the coefficients. ECMWF forecast data was chosen because it has been well validated against radiosonde observations collected by observation networks and stay within a range of one K from 100 to 1000 hPa (*Carminati et al.,* 2019; *Yan et al*., 2020). Variables associated with ECMWF data include temperature, vorticity, latitude, longitude, and time at 137 pressure levels. Observations were assimilated in daily ECMWF forecasts at 03:00, 09:00, 15:00, and 21:00 Coordinated Universal Time (UTC) to improve the accuracy of the forecasts (*Yan et al.,* 2020).

Chapter 3 Methodology

3.1 Data Quality Control

To ensure the ATMS data gathered from the CLASS website (https://www.avl.class.noaa.gov/saa/products/search?datatype_family=ATMS_TDR) was valid, the information had to be sorted to remove any erroneous entries. Quality control measures were performed on the dataset to prevent the analysis of brightness temperature from being skewed by invalid data. The first entries that needed to be removed were any measurement with incorrect geolocation data. Therefore, any data that contained latitude entries of less than -90° or greater than 90° were removed. Consequently, any recording of less than -180° or greater than 180° was also deleted. Additionally, any brightness temperature data points that were less than 0 K were masked, since Kelvin is an absolute scale that cannot be negative.

3.2 Application of Limb-Correction Algorithm

The equation used to apply limb-correction on the ATMS brightness temperature is given below as

$$\widehat{Tb(i,j)}_n = \overline{Tb(i)} + \sum_{i^a} a_{i^a j}(Tb(i^a, j) - \overline{Tb(i^a, j)}) \qquad (3.1)$$

where $\widehat{Tb(i,j)}_n$ is the estimated nadir brightness temperature at channel *i* at beam position *j*, where *n* denotes nadir. The predictand was chosen to be the average of brightness temperature of beam positions 48 and 49 at channel *i* to simulate nadir. $\overline{Tb(i)}$ is the expected value of brightness temperature in the training sample, which was saved into the coefficient files. When applying the limb-correction algorithm, an elevation dataset was used to differentiate land and water surfaces. This was required to determine whether or not either the land or water set of coefficients is used in the limb-correction algorithm. Channels 1 – 6 and 16 – 22 were separated into land and ocean

data points to calculate the two sets of coefficients, while coefficients calculated for ATMS channels 7 – 15 used all data points and were the same for both land and water coefficients (*Zhang et al.,* 2017).

3.3 Development of Visualization Tool

An overhaul of the Python script provided by NESDIS used to generate the brightness temperature plots was completed for this study. For a one-day global dataset of one satellite, the script took approximately 12 – 13 minutes instead of four hours to generate global plots for all 22 channels (about 8.5 minutes to apply the limb-correction and 4 minutes to generate the 22 plots). Due to this speed-up, the script was able to apply the S-NPP and NOAA-20 limb-correction algorithms in real-time for ongoing meteorological events, rather than purely focusing on past storms. As an example, global images produced by this script are shown in **Figures 3** and **4**.

In the new script, new gridding technique was used from the Satpy module called pyresample. The plots generated with this new re-gridding technique are shown in all of the figures below. This method works much more efficiently than the grid data function from matplotlib that was used previously and is one of the major contributors to the faster runtime of the new script. Also, pyresample includes the gaps in the data in the equatorial regions rather than interpolating over the gaps in the data, which is how the previous script handled the ATMS data.

Additionally, the script was updated to run with Python 3.7 and was modified to use Cartopy to plot the figures instead of Basemap. This is because both Python 2.7 and Basemap will not be supported past 2020. Additionally, the Satpy module has some built in functions to re-grid the data and transform the area file into a Cartopy-readable file, making it an efficient and logical choice to use with the Python script.

Moreover, vertical cross section and horizontal pressure level plotting capabilities were developed within the script. This tool allows the user to select a pressure level in the script based on the pressure levels retrieved using the temperature retrieval algorithm for clear and cloudy sky conditions (*Yan et al.,* 2020). Selecting pressure levels in the middle to upper troposphere in a tropical cyclone environment displays the horizontal distribution of the warm core in the center of the hurricane at that pressure level. A vertical cross section through the center of the tropical cyclone can also be taken, which provides a glimpse at the vertical structure of the warm core in the storm at a moment in time. Furthermore, datasets at different times can be used, which provides the capability of generating time series images of a hurricane of interest in real time. Examples of past storms this visualization tool was used for this study are shown in the following sections.

3.3 Retrieval of Temperature Field

The temperature profiles required for the surface pressure calculation were generated using the cloudy and clear sky coefficients provided by *Yan et al.* (2020). This study investigated the warm core of Hurricane Maria (2017), and used collocated ECMWF forecast data to generate the coefficients. These clear sky coefficients were calculated using multiple linear regression analysis using ECMWF forecast data and ATMS brightness temperatures for clear sky conditions over oceans between 55°N and 55°S. The regression analysis fit the ATMS data to the temperatures given by the ECMWF forecast output for specified pressure levels in the atmosphere. A set of clear and cloudy sky coefficients was required because of microwave contamination of low altitude ATMS channels that exist in precipitation regions. Cloudy sky regions were defined as areas where liquid water content (LWC) was greater than 0.1 mm.

***Table 2**: ATMS Temperature Retrieval Coefficients under Clear-Sky Conditions (Yan et al., 2020).*

Pressure (hPa)	C_0	C_5	C_6	C_7	C_8	C_9	C_{10}	C_{11}	C_{12}
100	320.6599	-0.10625	-0.60287	-1.25504	-0.15401	0.437027	0.847983	0.070333	0.527421
125	76.8446	-0.23747	-0.00492	-1.35077	0.207454	1.724383	0.565559	-0.11638	-0.0017
150	110.0501	0.012103	-0.14434	-0.52494	0.296516	1.445372	0.214832	-0.29531	-0.47922
175	30.96043	0.109432	-0.22209	-0.02049	0.51403	1.203924	-0.0507	-0.24891	-0.4509
200	-46.1608	0.079771	-0.26582	0.492909	0.652252	0.979259	-0.21599	-0.18971	-0.37338
225	-85.4314	0.077327	-0.23776	0.60195	0.877295	0.851982	-0.44682	-0.06387	-0.33001
250	-95.2567	0.017257	-0.15528	0.634539	1.019267	0.571366	-0.57653	0.019206	-0.15148
275	-117.135	0.055587	-0.08712	0.782818	0.892405	0.211403	-0.60053	0.093108	0.117308
300	-118.805	0.149316	-0.03517	0.931347	0.660616	-0.21839	-0.53303	0.131335	0.370222
350	-61.5821	0.358468	0.088906	0.951088	0.239775	-0.76446	-0.35917	0.124069	0.54591
400	9.36438	0.360768	0.222042	0.67234	0.186953	-0.58709	-0.26336	0.076691	0.240669
450	35.33472	0.152851	0.272103	0.560969	0.461841	-0.25445	-0.36459	0.067726	-0.04606
500	29.40022	-0.01046	0.384712	0.516798	0.486294	-0.13345	-0.34303	0.077119	-0.05952
550	63.96507	-0.10203	0.562661	0.383805	0.285932	-0.26698	-0.15297	0.108842	-0.01999
600	96.44167	-0.15317	0.788442	0.190916	0.025119	-0.30561	0.050787	0.124892	-0.03997
650	143.2692	-0.20692	0.708757	0.159597	-0.10422	-0.22256	0.113303	0.120785	-0.04482
700	181.6709	-0.1722	0.461591	0.227915	-0.16625	-0.16445	0.103596	0.09444	0.013294
750	202.8703	-0.23263	0.325728	0.367842	-0.19208	-0.12158	0.121035	0.039206	0.031266
800	198.314	-0.31497	0.287787	0.45067	-0.16858	0.006105	0.079429	-0.02965	0.071673
850	191.9804	-0.28721	0.208937	0.461531	-0.0573	0.108264	0.014017	-0.06003	0.034794
1000	280.7866	-0.03043	0.359284	0.122418	-0.16485	0.089945	0.152232	-0.05018	-0.44676

The coefficients derived for temperature retrievals under clear sky conditions are shown in **Table 2**. Under clear-sky conditions, the equation used to retrieve temperature from ATMS brightness temperature is given below as

$$T_{clear}(p) = C_0(p) + \sum_{i=5}^{12} C_i(p) T_b^{LC}(\nu_i), \tag{3.2}$$

where T_b^{LC} is limb-corrected brightness temperature. $T_{clear}(p)$ is the temperature value retrieved at a certain pressure level under clear-sky conditions. C_0 and C_i are the coefficients derived from the multiple linear regression analysis of collocated ECMWF analysis temperature fields with observed ATMS brightness temperature. These coefficients were calculated using ATMS brightness temperatures with the limb-correction algorithm applied to the dataset. Channels 5 – 12 were used to derive the coefficients because these channels have peaking heights in the middle to upper troposphere, based on the ATMS weighting functions calculated by the CRTM (**Figure 1**).

***Table 3**: ATMS Temperature Retrieval Coefficients under Cloudy-Sky Conditions (Yan et al., 2020).*

Pressure (hPa)	C_0	D_7	D_8	D_9	D_{10}	D_{11}	D_{12}
250	-19.2866	-0.19528	1.370933	0.734549	-0.53875	-0.2536	-0.04104
275	-27.7342	-0.15196	1.43145	0.694703	-0.62779	-0.22257	0.003358
300	-0.33316	-0.10131	1.438912	0.630412	-0.67269	-0.23788	-0.04269
350	68.51778	-0.02561	1.343275	0.53596	-0.62893	-0.37171	-0.12057
400	134.4448	-0.0647	1.151849	0.507469	-0.49661	-0.40876	-0.20721
450	167.106	-0.04602	0.967857	0.480291	-0.39855	-0.34592	-0.28507
500	163.2535	0.047036	0.80221	0.41908	-0.36971	-0.22907	-0.25659
550	171.2787	0.126816	0.543889	0.305135	-0.30659	-0.10995	-0.15667
600	158.0071	0.265367	0.147207	0.198768	-0.11688	-0.00302	0.001699
650	134.8896	0.26775	0.15195	0.363989	-0.05856	-0.15665	0.045391
700	160.2663	0.095645	0.309021	0.374669	-0.14726	-0.10289	-0.00517
750	174.0238	0.021106	0.32108	0.380357	-0.12783	-0.08021	-0.02893
800	197.1184	0.035897	0.273149	0.334336	-0.0716	-0.09296	-0.0822
850	223.2979	0.010666	0.260347	0.297613	-0.01861	-0.13007	-0.12532
1000	260.9304	0.119827	0.138551	0.103545	0.135816	-0.18666	-0.15321

The coefficients derived for temperature retrievals under cloudy sky conditions are shown in **Table 3**. Under cloudy-sky conditions, the equation used to retrieve temperature from ATMS brightness temperature is given below as

$$T_{cloudy}(p) = D_0(p) + \sum_{i=7}^{12} D_i(p) T_b^{LC}(\nu_i), \tag{3.3}$$

where T_b^{LC} is limb-corrected brightness temperature. $T_{cloudy}(p)$ is the temperature value retrieved at a certain pressure level under cloudy sky conditions. D_0 and D_i are the coefficients derived from the multiple linear regression analysis of collocated ECMWF analysis temperature fields with observed ATMS brightness temperature. Once again, these coefficients were calculated using ATMS brightness temperatures with the limb-correction algorithm applied to the dataset. Channels 7 – 12 were used to derive the coefficients to avoid microwave contamination from precipitation in the low to mid troposphere. A failure to account for this corruption of the microwave radiation

signal would lead to incorrect temperature retrievals in the atmosphere, skewing any analysis of interesting meteorological phenomenon.

Since Hurricanes Maria, Florence, and Dorian both occurred during the same time of year (late August/early September), just different years (2017, 2018, and 2019, respectively), it was assumed that the coefficients should be able to reasonably resolve the temperature field for Hurricanes Florence and Dorian. These coefficients were also used on Hurricane Michael, which occurred in October 2018. This is slightly later in the hurricane season than Florence and Dorian. The temperature retrieval coefficients were tested with Michael to see how well the warm core was resolved using the coefficients and data recorded by the ATMS instrument. A 0.1 mm cutoff was used for LWC, just like *Yan et al.* (2020) did in their paper to determine when to use cloudy coefficients vs. clear sky coefficients. Above 250 hPa, clear sky coefficients are used to retrieve temperature for both cloudy and clear sky locations. The cloudy coefficients act to remove the cold bias in the low and mid-levels of tropical cyclones that are caused by microwave contamination due to precipitation.

However, the temperature retrieval algorithm does experience significant errors for hurricanes in close proximity to the coast. This is due to radiation contamination from land surfaces. Since the retrieval coefficients were calculated using datasets over the oceans, the introduction of land contamination causes large biases in the temperature retrieval. Therefore, temperature retrievals conducted in the manner of this study struggle to resolve accurate meteorological features that are located close to the coastline.

3.4 Surface Pressure Tendency

Surface pressure tendency was calculated using the vertical temperature profiles retrieved using the techniques from the previous section combined with the hydrostatic equation. Based on

the principles of the hydrostatic equation, warm air columns will produce low surface pressure, while cold air columns will produce high surface pressure. Therefore, the development of the upper-level warm cores that exist in intense tropical cyclones will lead to pressure changes at the surface below the warm core. The hydrostatic equation was incorporated into this study of ATMS brightness temperature by using the equation below

$$p_s = p(z_t) \exp\left(\frac{g}{R}\int_{z_b}^{z_t} T^{-1} dz\right), \tag{3.4}$$

which integrated the atmospheric column from the top of the atmosphere to the surface to calculate surface pressure. In this equation, p_s represents surface pressure, $p(z_t)$ is the pressure at the top of the atmospheric column, g is the gravitation acceleration (9.8 m/s2), Δz is the distance in meters between two pressure levels, R is the gas constant of dry air (287 J/kg*K.

In this calculation, an estimate of surface pressure was not required to find surface pressure tendency using retrieved ATMS temperature. The Δz parameter was estimated using an interpolation of the vertical heights and pressure levels of the Jordan mean tropical sounding with the pressure levels associated with the temperature retrieval from ATMS brightness temperatures. This Jordan sounding is an average of vertical temperature and humidity profiles taken in the West Indies region during "hurricane season", which was arbitrarily chosen to be between July and October (*Jordan,* 1958). The mean temperature and relative humidity profiles for the associated heights and pressure levels is shown in **Table 4**. An interpolation of the Jordan sounding with retrieved temperatures at pre-determined pressure levels was used primarily to estimate the distance between two pressure levels. This was required because the pressure levels of the Jordan sounding and retrieved temperature from ATMS brightness temperature were not the same. The interpolation was achieved using the one-dimensional interpolation function

provided by the SciPy module in Python. Pressure at the top of the atmospheric column, $p(z_t)$, was chosen to be 100 hPa, since this is the highest pressure level that temperature retrievals were calculated. This allowed for the vast majority of the mass in the atmospheric column to be below z_t, leading to reasonable surface pressure tendency values.

***Table 4**: Mean temperature and relative humidity sounding data (Jordan sounding) for the West Indies area during "hurricane season" (July – September) (Jordan, 1958).*

Pressure Level (hPa)	Height (m)	Temperature (°C)	Relative Humidity (%)
30	23971	-54	-
40	22139	-57.3	-
50	20743	-60.6	-
60	19620	-63.9	-
80	17883	-69.8	-
100	16568	-73.5	-
125	15260	-72.2	-
150	14177	-67.6	-
175	13236	-61.5	-
200	12396	-55.2	-
250	10935	-43.3	-
300	9682	-33.2	-
350	8581	-24.8	-
400	7595	-17.7	-
450	6703	-11.9	42
500	5888	-6.9	45
550	5138	-2.5	47
600	4442	1.4	50
650	3792	5.1	54
700	3182	8.6	57
750	2609	11.8	61
800	2063	14.6	68
850	1547	17.3	74
900	1054	19.8	79
950	583	23.0	81
1000	132	26.0	81
1015.1	0	26.3	84

It is important to note that this methodology does have limitations in calculating surface pressure tendency in tropical cyclones. The temperature retrieval pressure levels were defined between 1000 and 100 hPa to calculate coefficients between ATMS brightness temperature and

co-located ECMWF temperature profiles. The retrieved surface pressure tendency needs the entire column of retrieved temperature to accurately calculate the surface pressure. The surface pressure was very inaccurate when only a portion of the column to a lower pressure (such as in a hurricane) was used to calculate surface pressure. This is because the next pressure level above 1000 hPa is 850 hPa, which is too low to use for the center of a hurricane. Therefore, it seemed reasonable to calculate the pressure all of the way down to 1000 hPa and the results, described in detail in the next section, seem to support this method. However, this is an issue that can be addressed in the future when unique coefficients are calculated for each storm case.

Another issue with this method is related to how the Jordan sounding was used to estimate the distance between the two pressure levels. This sounding is based on the average of data collected in the Caribbean region during the months of the hurricane season. The results shown in the next section were found using an interpolation of the heights and pressure levels shown in **Table 4** with the associated pressure levels of the temperature retrieved from ATMS brightness temperature data. However, this is a limitation of the study since the vertical distances between pressure levels are not the constant values found in the Jordan sounding, since atmospheric profiles are constantly changing. This would be another area of improvement for future work to improve the results of this study.

Chapter 4 Results

4.1 Visualization Tool

A visualization tool was required to investigate interesting weather phenomenon in a dataset of limb-corrected ATMS brightness temperature. This tool needed to have the capacity to display results for user analysis to assist in real time forecasting. The visualization method developed in this study allows the user to plot global and regional images of limb-corrected brightness temperature. Furthermore, it also has the capability to plot vertical cross sections of retrieved temperature values and can calculate and plot surface pressure based on the retrieved temperature in the atmospheric column. These extra analysis features are presented in greater detail in later sections.

Plots of original and limb-corrected brightness temperature for the ATMS instrument on the Suomi-NPP and NOAA-20 satellites are shown in **Figure 3** and **Figure 4**, respectively. ATMS channels 4 and 8 are shown for the Suomi-NPP and NOAA-20. It is immediately clear from the figures what the impact of the limb-correction is on the dataset. Prior to the application of the limb-correction algorithm, ATMS brightness temperature is displayed with many banding errors due to the consequences of the limb effect. This is shown in the left figures of both **Figure 3** and **Figure 4**. To compensate for this error, the limb-correction algorithm removes this bias and smooths out the banding to plot accurate retrievals of brightness temperature in the atmosphere. The result of applying the correction algorithm to ATMS brightness temperature is shown in the right plots of **Figure 3** and **Figure 4**.

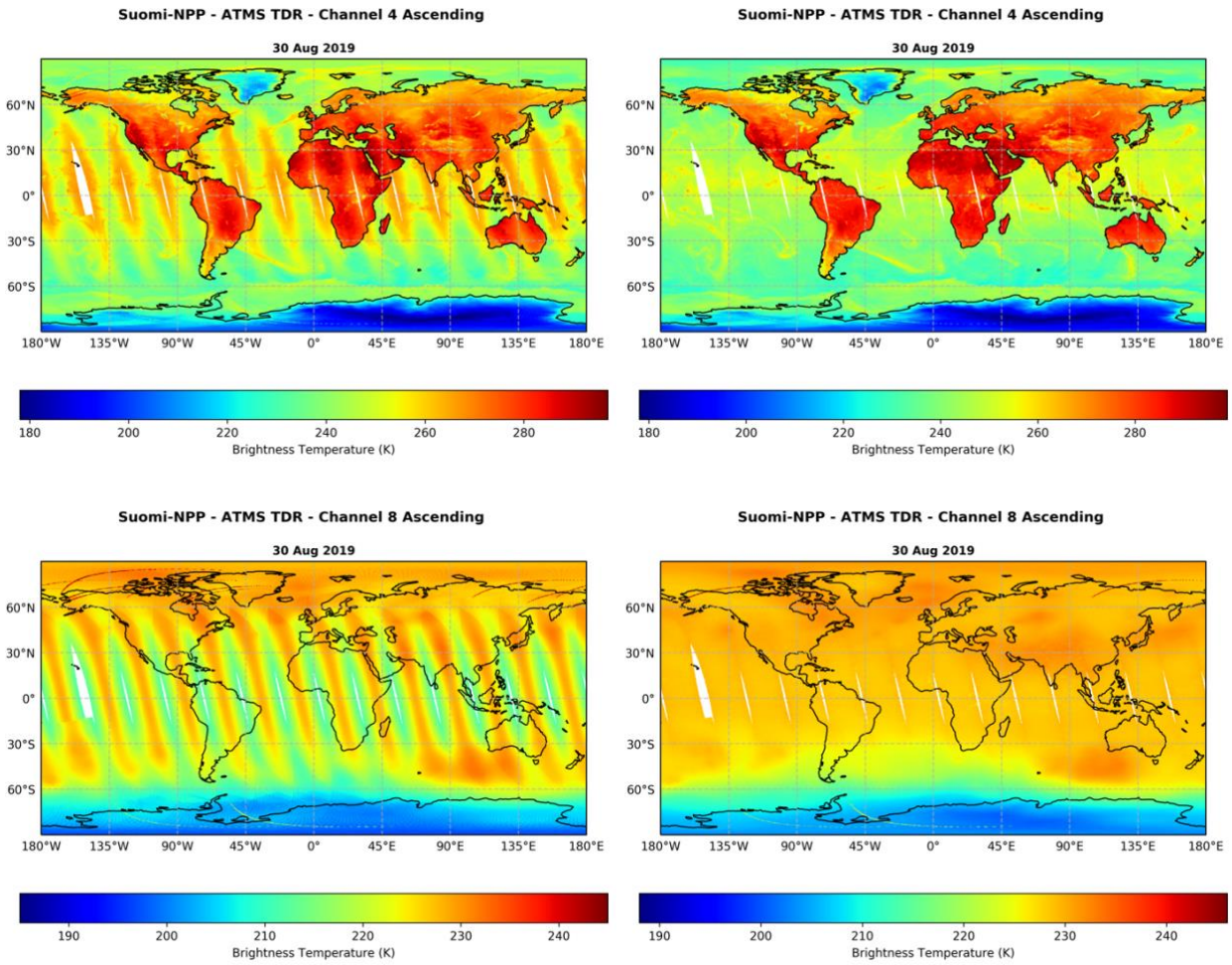

Figure 3*: Plots of Suomi-NPP ascending node ATMS data showing channels 4 (top) and 8 (bottom) with both original retrievals (left) and limb-corrected brightness temperature (right) for data collected on August 30, 2019.*

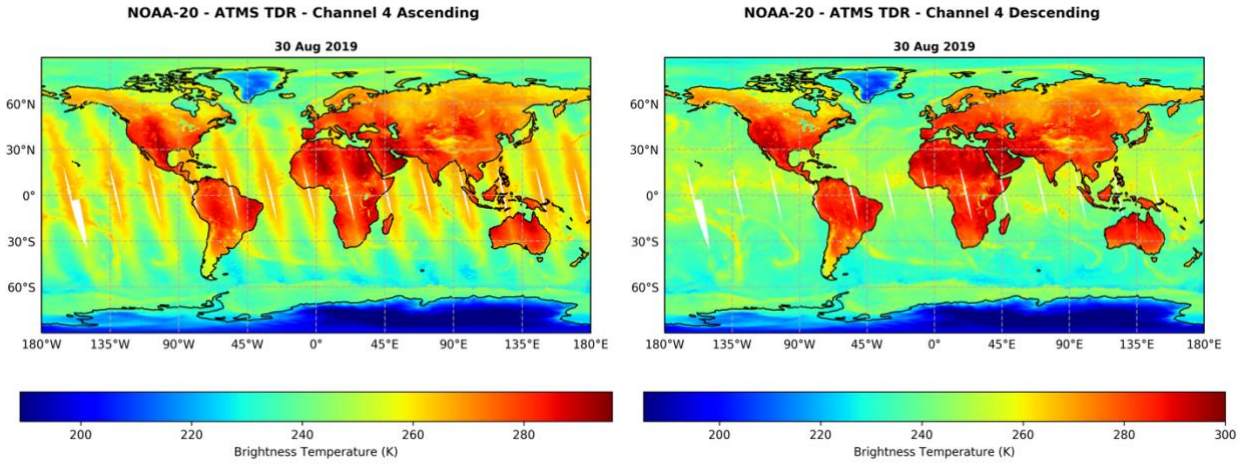

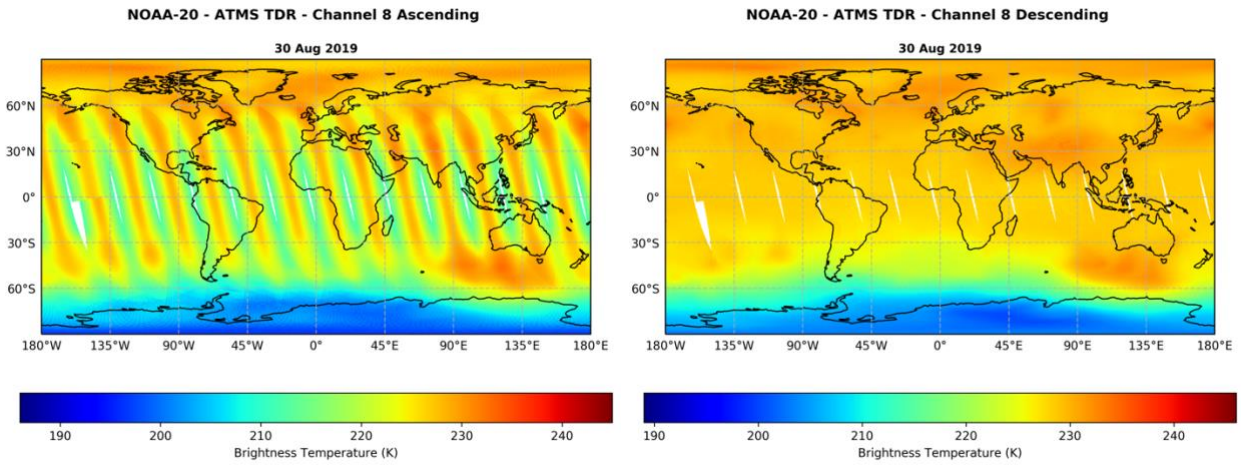

Figure 4*: Plots of NOAA-20 ascending node ATMS data showing channels 4 (top) and 8 (bottom) with both original retrievals (left) and limb-corrected brightness temperature (right) for data collected on August 30, 2019.*

The limb effect is obvious for both ATMS channels 4 and 8 plotted in **Figure 3** and **Figure 4**. This bias is apparent in all 22 channels for the ATMS instrument for both the Suomi-NPP and NOAA-20 satellites. Limb correction is a critical step in data processing to allow for studies of interesting meteorological phenomenon using ATMS brightness temperature, such as the upper-level warm cores of tropical cyclones. Small gaps in the data are also visible in the equatorial regions in **Figure 3** and **Figure 4**. Gaps exist in equatorial regions where the ATMS scans fail to completely overlap each orbital pass to provide complete spatial coverage of the Earth's surface.

4.2 Retrieved Temperature Field

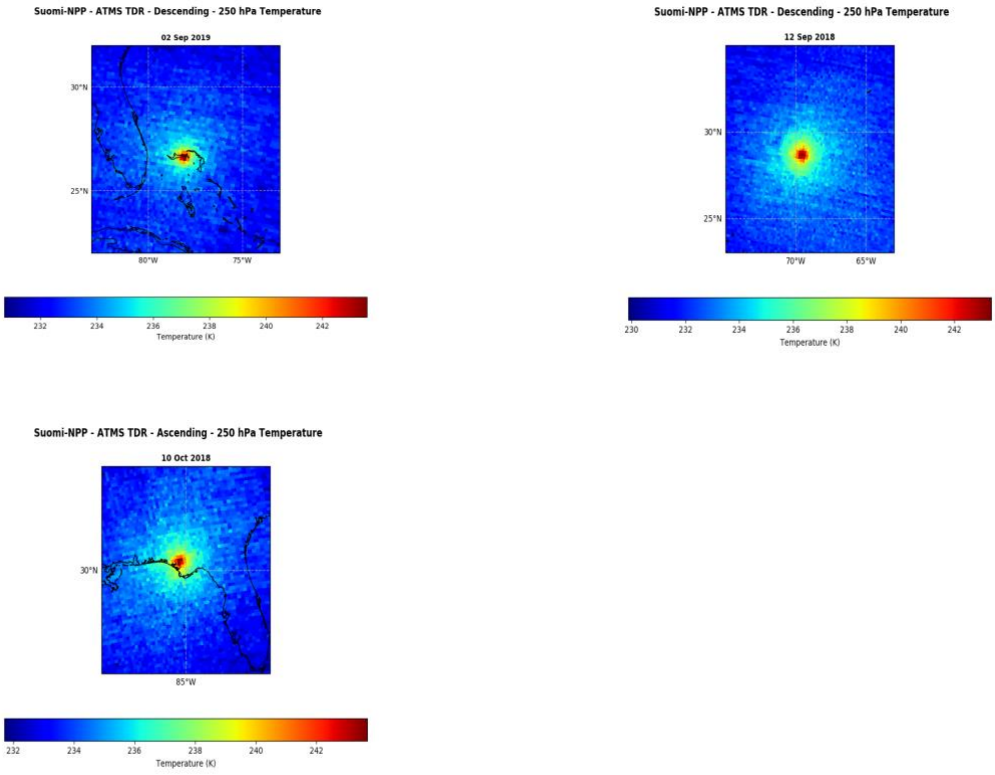

Figure 5*: Retrieved temperature field at 250 hPa from Suomi-NPP ATMS data at peak intensity of Hurricanes Dorian (top left), Florence (top right), and Michael (bottom left).*

Retrieved temperature fields calculated using limb-corrected ATMS brightness temperature are shown in **Figure 5**. This figure showcases the maximum time of maximum intensity of the upper-level warm core at the 250 hPa level for Hurricanes Dorian (top left), Florence (top right), and Michael (bottom left). A pressure level of 250 hPa is shown because this was the height at which the most intense warm core values were retrieved from the ATMS brightness temperature datasets. The plots in **Figure 5** clearly show an intense warm temperature anomaly at 250 hPa for all three storms. Observations from the tropical storm reports (*Beven II et al.*, 2019; *Stewart et al.*, 2018) and advisory data reveal that both Hurricanes Dorian and Michael reached category 5 intensity on the Saffir-Simpson hurricane wind scale, with Hurricane Florence

slightly weaker as a category 4 hurricane at peak intensity. The strength of these tropical cyclones suggests the presence of a strong upper-level warm core, which is exactly what is displayed in **Figure 5**. Also, Hurricanes Dorian, Florence, and Michael all experienced a period of rapid intensification immediately prior to attaining peak intensity (*Beven II et al.*, 2019; *Stewart et al.*, 2018). This rapid surface pressure drop is significantly driven by the development and intensification of the upper-level warm core (*Zhang and Chen*, 2012). The presence of strong upper-level warm cores in **Figure 5** indicates that the temperature retrieval process was able to resolve the warm temperature anomaly generated during a period of rapid intensification.

4.3 Time Evolution of Upper-Level Warm Core

Figure 6 shows vertical cross sections through Hurricane Dorian of the anomalous temperature field for Suomi-NPP descending node ATMS data from 29 August – 4 September 2019. The development of the upper-level warm core is apparent as the storm intensifies, particularly on August 30th and all times after. This shows that the temperature retrieval using the coefficients provided by *Yan et al.* (2020) was able to resolve the upper-level warm core of Hurricane Dorian. The intensity of the warm core also strongly correlates with the surface pressure of Dorian (*Zhang and Weng*, 2012). Initially, the upper-level warm core strengthened by about 3 K between August 29th and September 1st as the storm intensified into a category 3 hurricane while moving away from Puerto Rico. At this point, Hurricane Dorian experienced a period of rapid intensification that quickly deepened its upper-level warm core by approximately 7K between September 1st and September 2nd. This coincides with the period of rapid intensification Dorian underwent during this time, strengthening to a very intense category 5 hurricane on September 2nd, with a minimum surface pressure of 914 hPa. In **Figure 6**, the warm core on September 2nd reached a maximum of 15.82K at the time of maximum intensity.

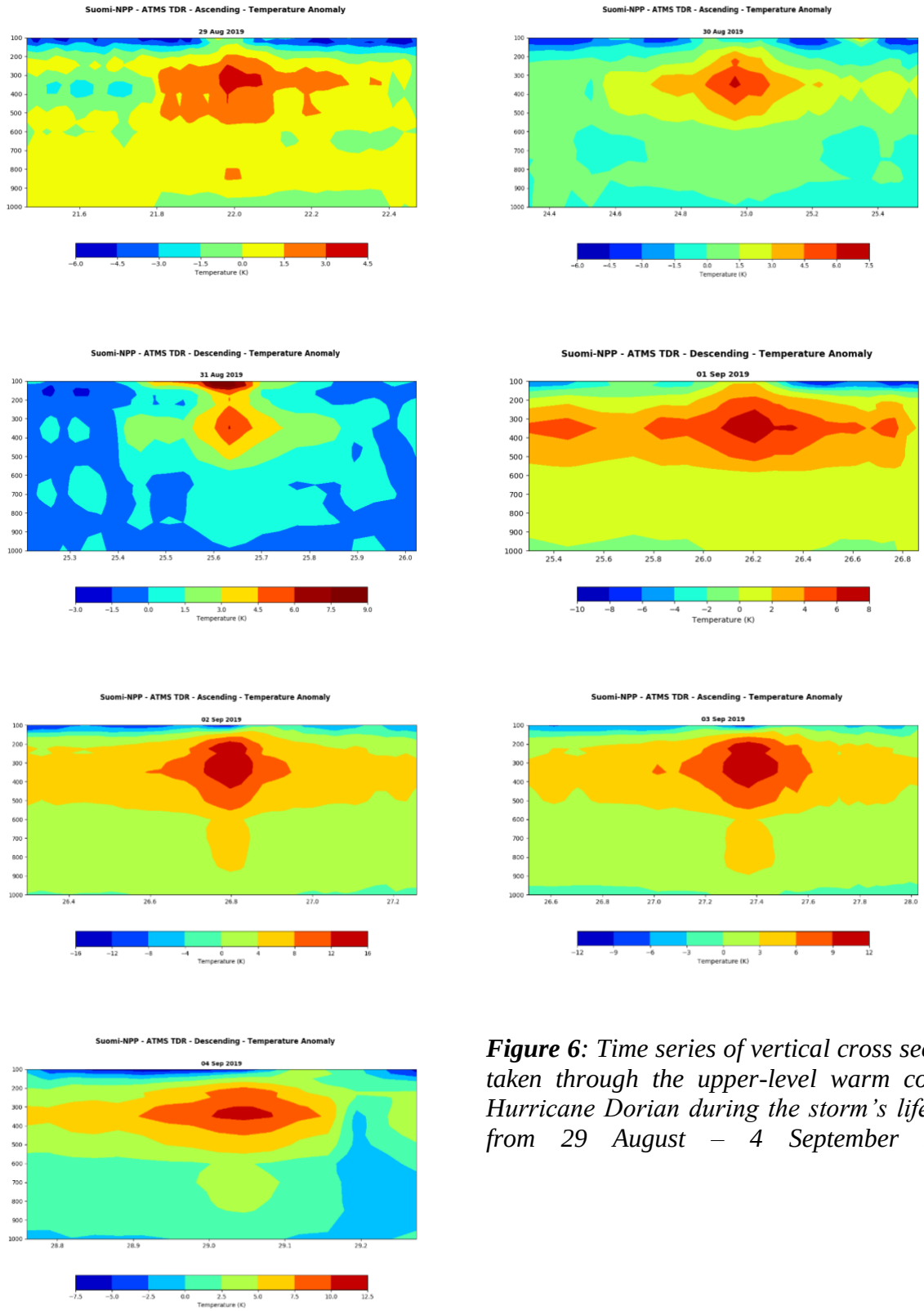

Figure 6*: Time series of vertical cross sections taken through the upper-level warm core of Hurricane Dorian during the storm's lifecycle from 29 August – 4 September 2019.*

Vertical cross sections of the anomalous temperature field were also taken of hurricane Florence to investigate the time evolution of the upper-level warm core. **Figure 7** shows how the warm core intensified and weakened during the life cycle of the tropical cyclone. The presence of the strongest warm core during the time period on September 12th correlates with the time that Florence reached its maximum intensity based on its tropical storm report (*Stewart and Berg*, 2018). Hurricane Florence reached a minimum surface pressure of 943 hPa on September 12th, with a maximum warm core temperature anomaly of 14K. Hurricane Florence experienced two intensification and weakening periods between the time period of the study, September 4th – September 14th (*Stewart and Berg*, 2018). The warm core reached its first maximum of 8.85K on September 5th, which was the time Florence reached its first intensity peak, with a minimum surface pressure of 958 hPa based on the advisory data. Florence then weakened considerably from September 5th to September 7th into a tropical storm and its warm core cooled by about 3K, which is shown in **Figure 7**. The warm core remained in a relatively steady state until September 8th, with little change in intensity. After this time, from September 8th through September 12th, the warm core steadily intensified, warming about 8 K. Following this secondary peak in intensity, the warm core once again begins to weaken, signaling the weakening trend observed in the tropical cyclone report (*Stewart and Berg*, 2018). However, a discrepancy exists in **Figure 7** on September 14th, which shows the warm core intensifying when the storm was shown to be weakening based on observations. This inconsistency was most likely caused by Hurricane Florence's proximity to land, which likely introduced errors into the temperature retrieval algorithm.

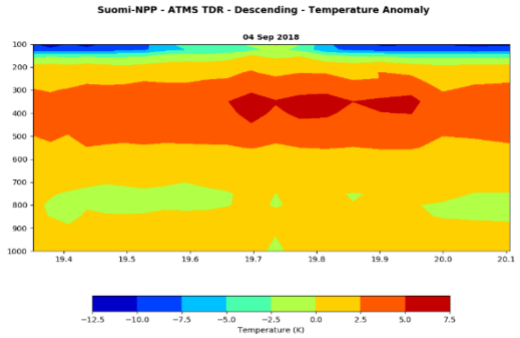
Suomi-NPP - ATMS TDR - Descending - Temperature Anomaly
04 Sep 2018
Temperature (K)

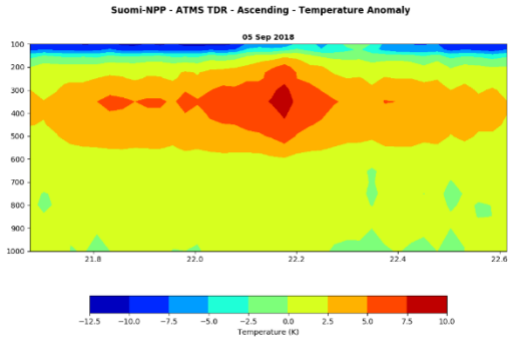
Suomi-NPP - ATMS TDR - Ascending - Temperature Anomaly
05 Sep 2018
Temperature (K)

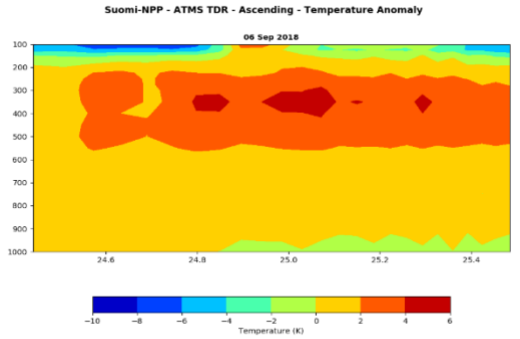
Suomi-NPP - ATMS TDR - Ascending - Temperature Anomaly
06 Sep 2018
Temperature (K)

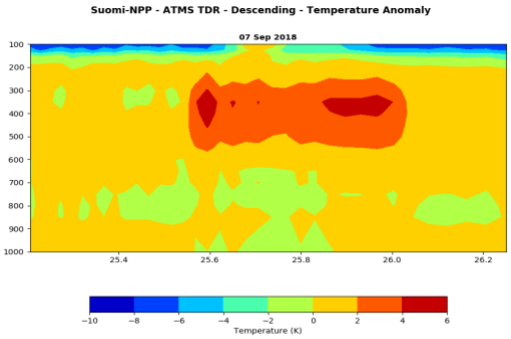
Suomi-NPP - ATMS TDR - Descending - Temperature Anomaly
07 Sep 2018
Temperature (K)

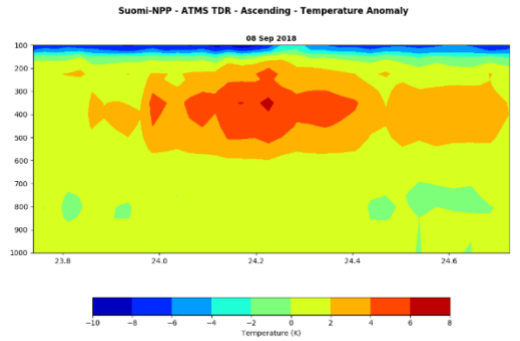
Suomi-NPP - ATMS TDR - Ascending - Temperature Anomaly
08 Sep 2018
Temperature (K)

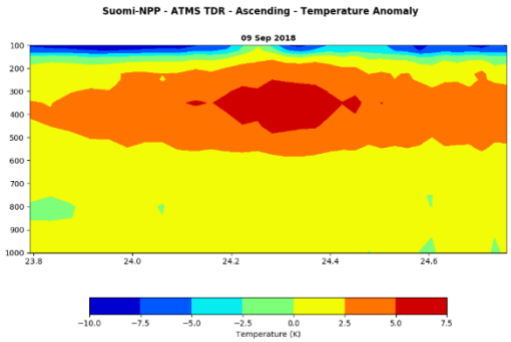
Suomi-NPP - ATMS TDR - Ascending - Temperature Anomaly
09 Sep 2018
Temperature (K)

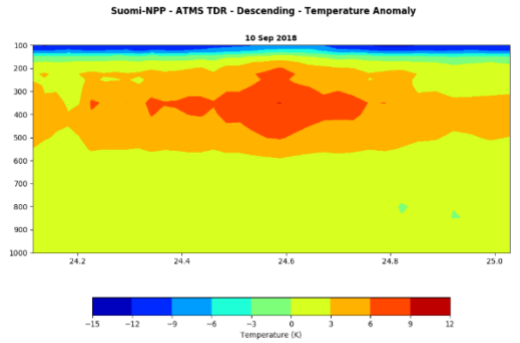
Suomi-NPP - ATMS TDR - Descending - Temperature Anomaly
10 Sep 2018
Temperature (K)

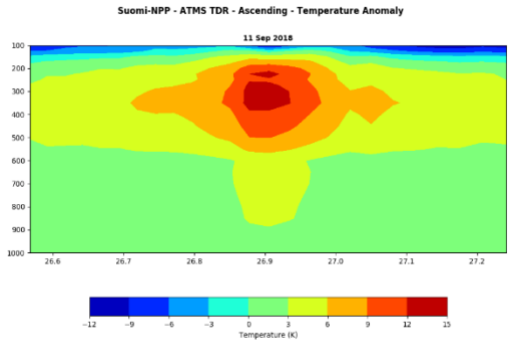
Suomi-NPP - ATMS TDR - Ascending - Temperature Anomaly
11 Sep 2018
Temperature (K)

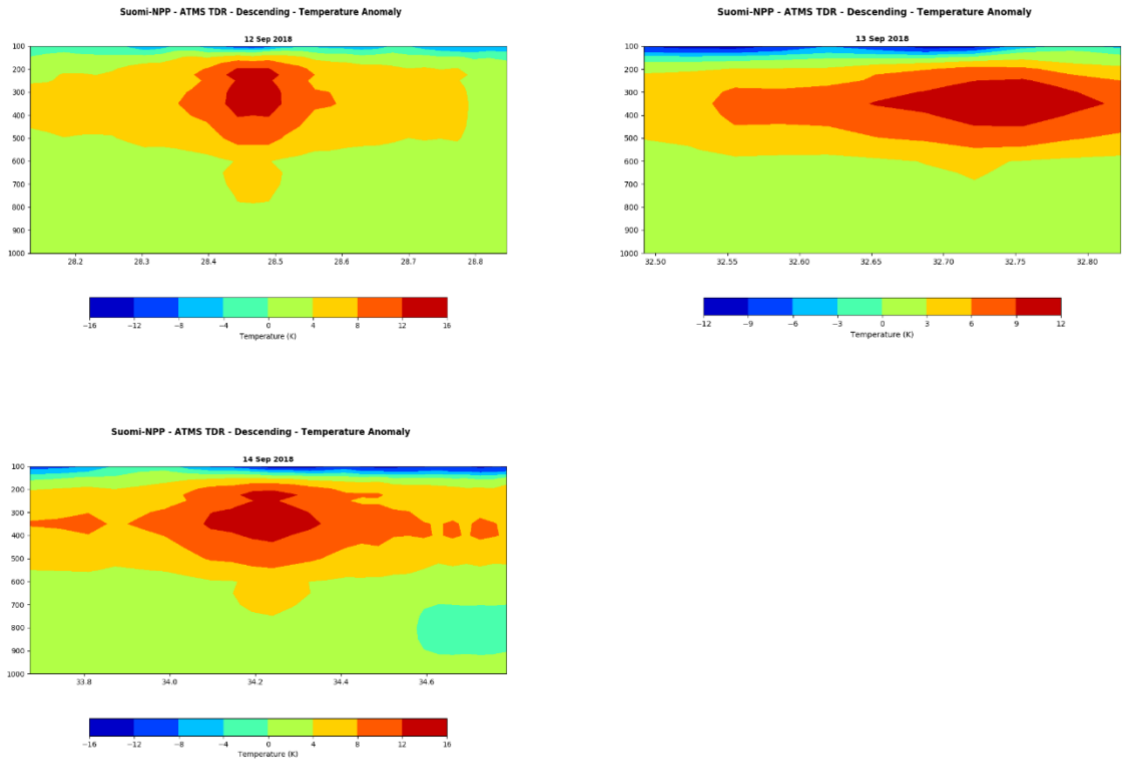

Figure 7*: Time series of vertical cross sections taken through the upper-level warm core of hurricane Florence during the storm's lifecycle from 4 – 14 September 2018.*

A third tropical cyclone case that was analyzed was Hurricane Michael, which occurred in October 2018. **Figure 8** shows how the warm core intensified as Michael rapidly intensified in the Gulf of Mexico. From the time of its development on October 7th, hurricane Michael strengthened up to the time of its landfall as a category 5 hurricane on October 10th. The presence of the strongest warm core on this date correlates with the time that Michael reached its maximum intensity based on the advisory data. Hurricane Michael reached a minimum surface pressure of 919 hPa (*Beven II et al.*, 2019), with a maximum warm core temperature anomaly of 14.35K. Michael experienced a rapid intensification period during the time of this study. Rapid intensification was especially significant on October 9th and October 10th based on the tropical cyclone report (*Beven II et al.*, 2019). This rapid intensification period coincides with the intensification of the upper-level warm

core, as the warming aloft contributed to the deepening of surface pressure (*Zhang and Chen*, 2012). The time period for this study was stopped on October 10th because Michael made landfall on that date. Temperature retrieval errors would have been introduced once the storm was in close proximity to the coast and this would have caused incorrect depictions of the evolution of the warm core as it weakened over land.

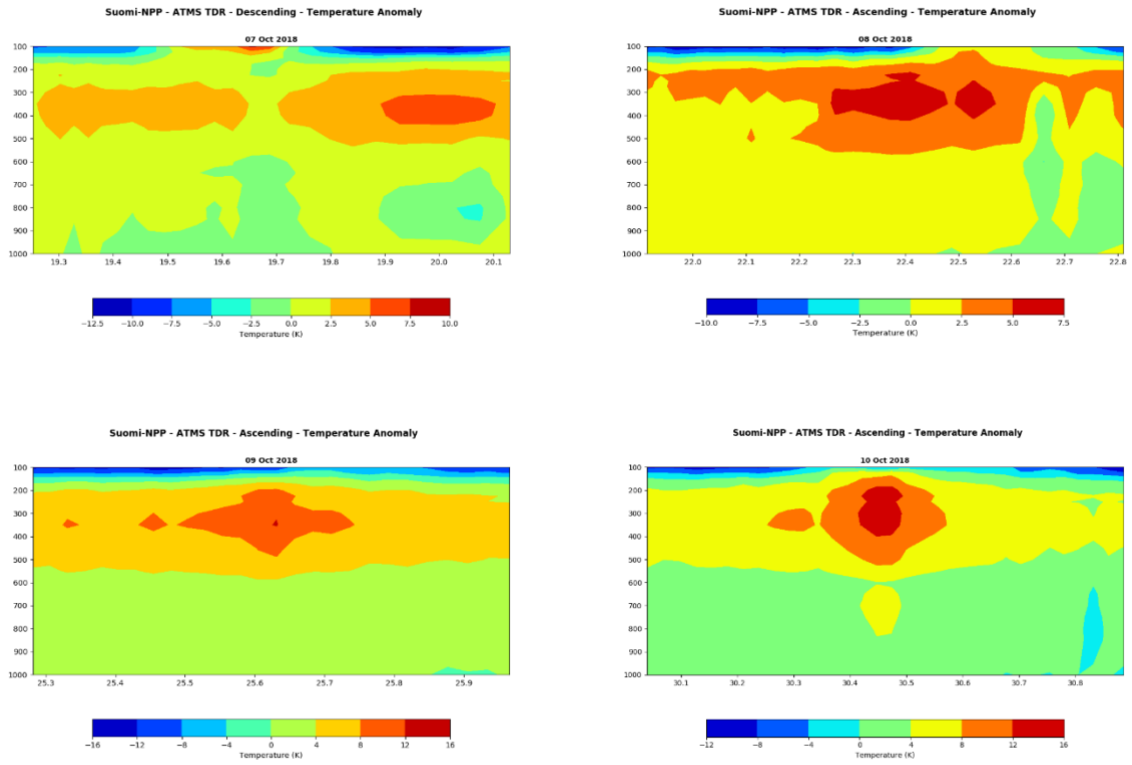

***Figure 8**: Time series of vertical cross sections taken through the upper-level warm core of hurricane Michael during the storm's lifecycle from 7 – 10 October 2018.*

4.4 Tropical Cyclone Surface Pressure Tendency

Using the temperature retrieval algorithm and coefficients from *Yan et al.* (2020), surface pressure plots were created of Hurricane Dorian. The lowest surface pressure calculated using the hydrostatic equation and the retrieved temperatures is compared with the best track surface pressure data in **Figure 9**. This figure shows the evolution of the minimum surface pressure of

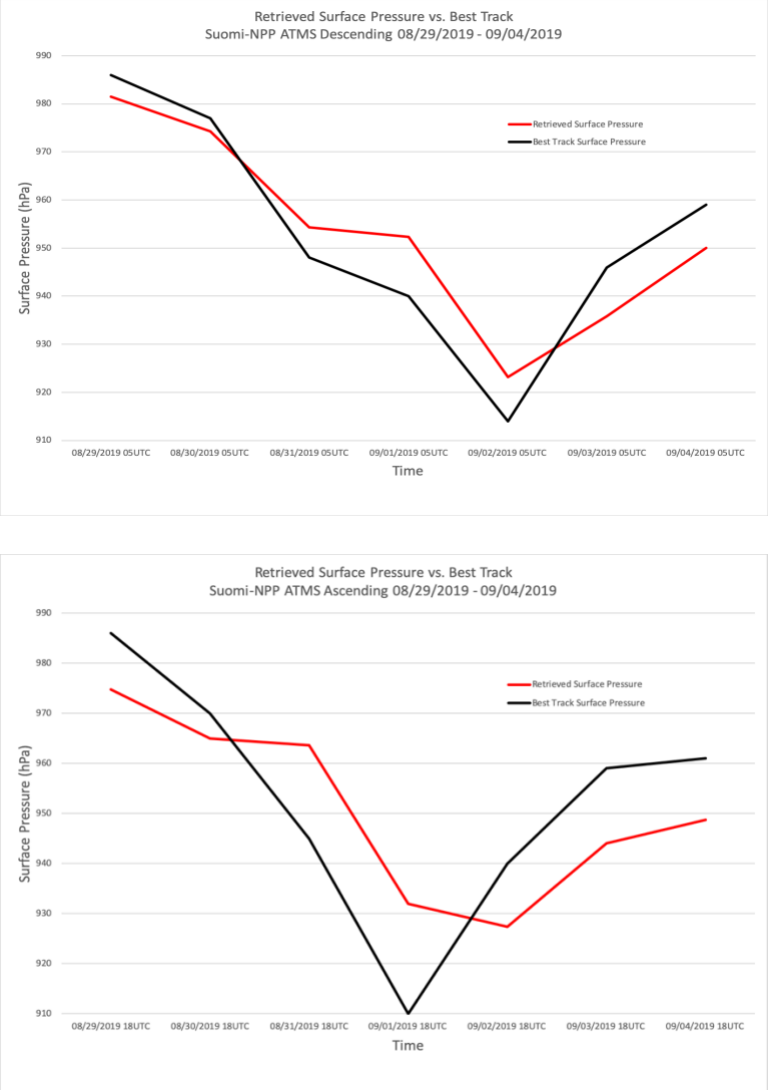

***Figure 9**: Plot of surface pressure calculated with temperature retrieved from Suomi-NPP ATMS brightness temperature descending node (top), ascending node (bottom), and best track surface pressure data for Hurricane Dorian from 29 August – 4 September 2019.*

Hurricane Dorian with data collected from the descending node (top plot) and ascending node (bottom plot) of Suomi-NPP ATMS instrument from 29 August to 4 September 2019. The top plot of **Figure 9** shows that the tendency of the calculated surface pressure from ATMS descending node compares well with the surface pressure from the advisory data. However, the ascending node does not follow the pressure tendency quite as well as the descending node. This is because there were more times when the center of Hurricane Dorian was located near the edge of the

satellite scan in the ascending node of the dataset (bottom plot) vs. the descending node (top plot). Therefore, larger biases at the edge of the scan contributed to the incorrect pressure tendencies. However, once the hurricane moved away from the edge of the satellite scan, the surface pressure calculation was once again able to capture the surface pressure tendency reasonably well.

Best track advisory data of Hurricane Dorian from the National Hurricane Center in **Figure 9** shows the storm intensifying from August 29th until reaching peak intensity on September 2nd. Periods of rapid intensification occurred between August 30th and August 31st and September 1st and September 2nd. This deepening of surface pressure can also be seen in **Figure 10**, which showcases how the low pressure center of Hurricane Dorian deepened as it approached the northern Bahamas. Hurricane Dorian then made landfall in the Abaco Islands and Grand Bahama Island on September 2nd and almost completely stalled over the northern Bahamas. This led to a weakening trend after the time of landfall as Dorian upwelled cooler ocean water and experienced disruption of its inner structure due to being over Grand Bahama Island for over 24 hours. Dorian then slowly moved parallel to the east coast of Florida and was able to reduce its rate of weakening as it moved back over open water and warmer ocean temperatures (see **Figures 9** and **10**).

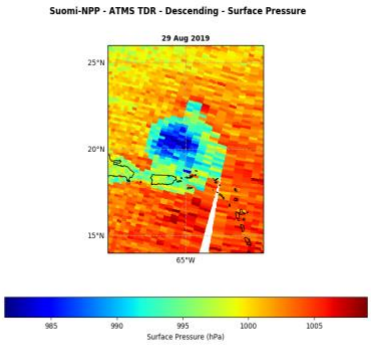

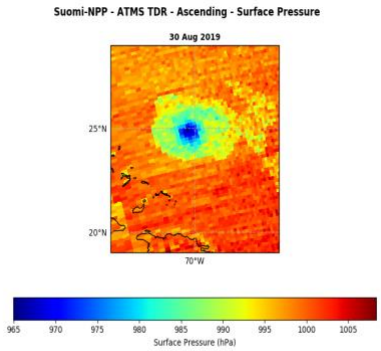

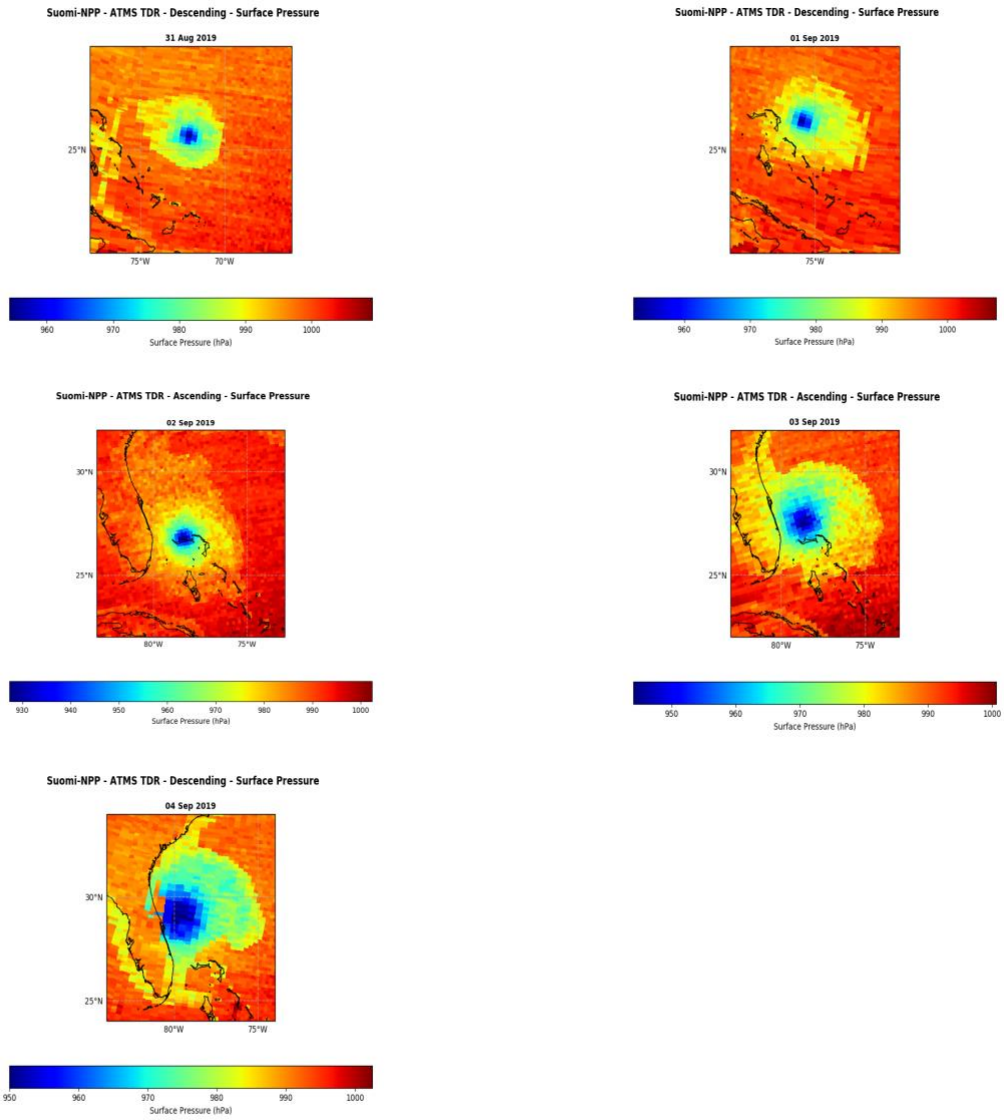

Figure 10*: Daily time series pressure plots of Hurricane Dorian derived from ATMS brightness temperature from 29 August – 4 September 2019.*

Additionally, surface pressure plots were created of Hurricane Florence. The surface pressure calculated at Florence's location using the hydrostatic equation and the retrieved temperatures is compared with the best track surface pressure data in **Figure 11**. This figure highlights the evolution of the minimum surface pressure of hurricane Florence with data collected from the ascending node of the Suomi-NPP ATMS instrument from September 4, 2018 to September 14, 2018. The figure shows the calculated pressure tendency is reasonable for most of

the time period, except for days where the center of the hurricane is near the edge of the satellite scan, such as 7 September 2018. However, the calculated pressure is usually lower than the best track surface pressure for the majority of the time period. This is most likely because the temperature retrieval is causing the warm core to be warmer than it should be, causing the lower calculated pressures. Also, the different pressure tendency observed between September 13th and September 14th in **Figure 11** is due the proximity of Florence to the coast, which is causing errors to occur in the temperature retrieval.

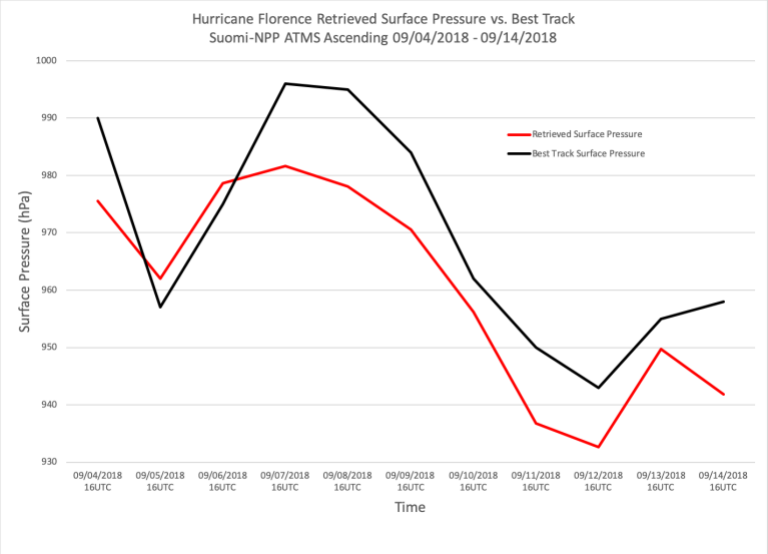

Figure 11*: Plot of surface pressure calculated with temperature retrieved from Suomi-NPP ATMS brightness temperature ascending node and best track surface pressure data for hurricane Florence during 4 – 14 September 2018.*

It is clear from **Figure 11** that there were two periods of intensification and weakening for hurricane Florence. This can also be seen in **Figure 12**, displaying visual depictions of the time evolution of surface pressure inside hurricane Florence. The first peak in intensity was reached on September 5, 2018 in both the advisory data from the tropical cyclone report (*Stewart and Berg*, 2018) and the surface pressure calculated using temperature retrieved from ATMS brightness temperature. A weakening period then occurs in both best track and retrieved surface pressure. This can be seen from September 6th through September 8th (**Figure 12**), where the pressure field

becomes more diffuse and higher minimum pressure values exist. However, the retrieved surface pressure fails to rise to the levels observed by the advisory data. Instead, the pressure remains about 15 hPa below what was reported in the best track data (*Stewart and Berg*, 2018). Once the hurricane enters its second period of intensification on September 8, 2018, the retrieved and best track surface pressure once again start to converge on similar values, while also having the same trend of decreasing surface pressure. Both eventually reach a maximum intensity on September 12, 2018, with the retrieved surface pressure being about 10 hPa lower than the surface pressure reported in the advisory data (*Stewart and Berg*, 2018). This strong low pressure center is especially apparent in **Figure 12** on September 11th and September 12th. On these dates, the low surface pressure center is very intense and tightly clustered near the center, which signifies the presence of a strong upper-level warm core aloft.

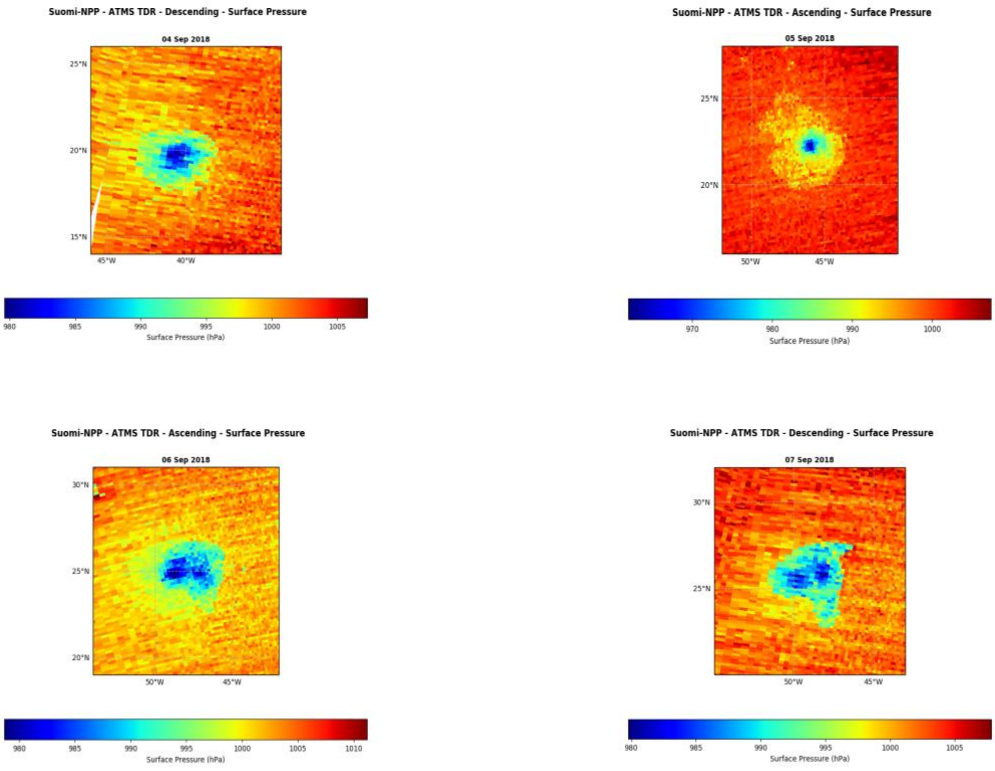

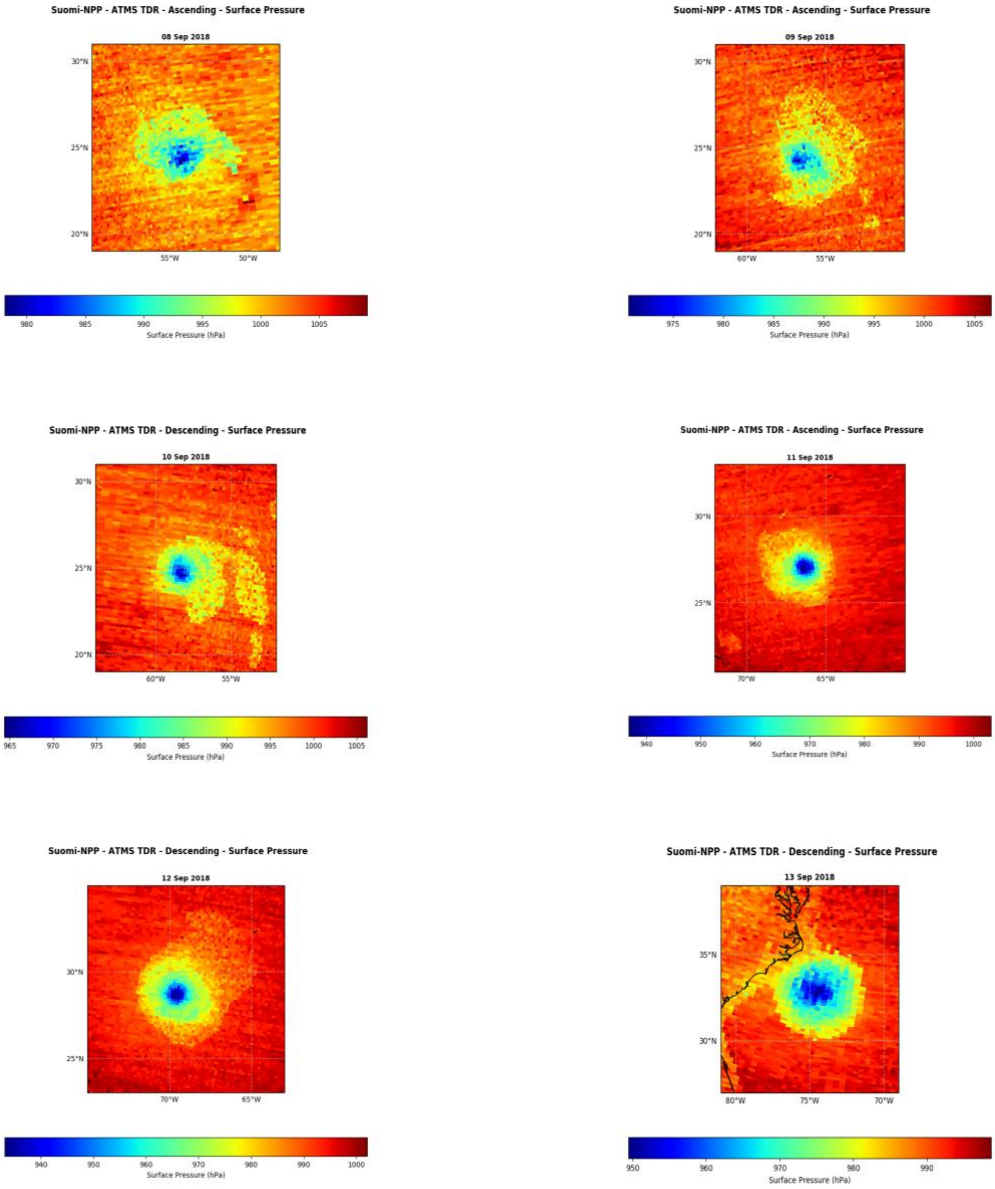

***Figure 12**: Daily time series pressure plots of hurricane Florence derived from ATMS brightness temperature during 4 – 14 September 2018.*

The same procedure of temperature retrieval and pressure calculation were used to create surface pressure plots of hurricane Michael. The lowest surface pressure calculated using the hydrostatic equation and the retrieved temperatures is compared with the best track surface pressure data in **Figure 13**. This figure shows the evolution of the minimum surface pressure of hurricane Michael with data collected from the descending node (top plot) and ascending node (bottom plot) of Suomi-NPP ATMS instrument during 7 – 10 October 2018. Both figures show that the calculated pressure tendency is reasonable for most of the time period, particularly on October 9th and October 10th. However, the calculated pressure at the beginning is much lower than the best track surface pressure in both plots. A possible reason for this is that the temperature retrieval may have exaggerated the strength of the upper-level warm core, which would have caused the pressure calculated to be much lower than it should be. Another possible reason is that hurricane Michael was close to land during its development, which would have caused errors in the temperature retrieval, leading to incorrect surface pressure calculations (*Yan et al.,* 2020). However, once the hurricane is rapidly intensifying away from land in the middle of the Gulf of Mexico, the calculated surface pressure tendency of Michael tracks very well with the surface pressure tendency provided by the advisory data. This can be seen in both plots in **Figure 13**, where the surface pressure tendency shows rapid deepening up to Michael's landfall as a category 5 hurricane in Florida.

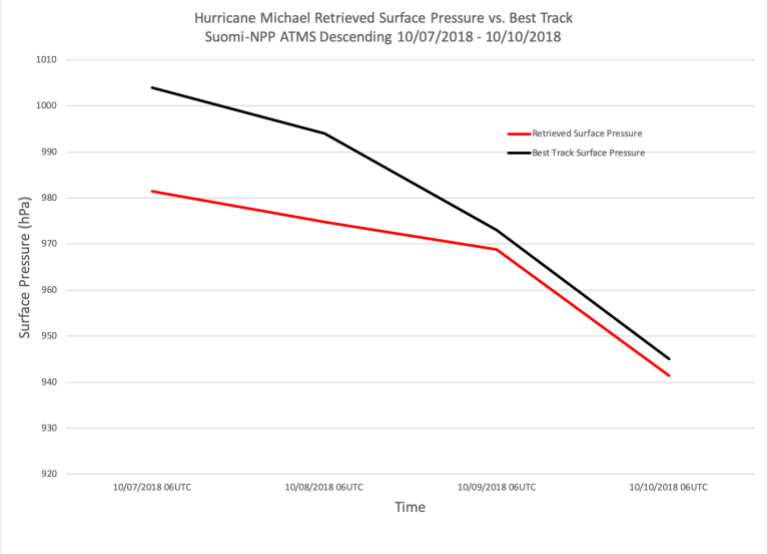

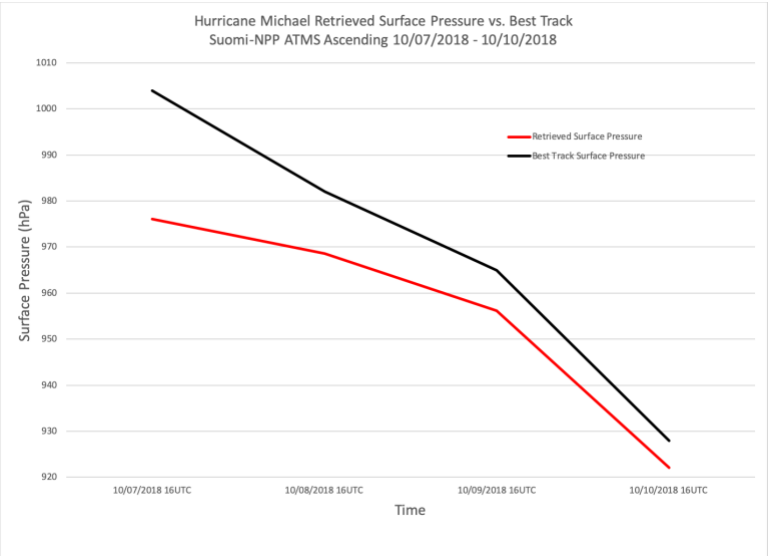

Figure 13*: Plot of surface pressure calculated with temperature retrieved from Suomi-NPP ATMS brightness temperature descending node and best track surface pressure data for hurricane Michael during 7 – 10 October 2018.*

Figure 13 clearly shows there was a period of steady and rapid intensification prior to Michael's landfall in the Florida panhandle. This intensification is visually highlighted in **Figure 14**, which displays the time evolution of surface pressure as hurricane Michael moved across the Gulf of Mexico. Hurricane Michael initially strengthened slowly into a tropical storm between October 7th and October 8th. The weaker nature of Michael at this time is visible in **Figure 14**, which shows Michael's pressure field as relatively weak and diffuse on these dates. However, a

period of rapid intensification followed on October 8th and continued up to landfall on October 10th. Hurricane Michael's pressure field in **Figure 14** on October 9th and October 10th reflects this period of strengthening recorded in the tropical cyclone report (*Beven II et al.,* 2019). In these plots, the surface pressure of Michael deepens significantly, and the structure becomes more compact and concentrated. This is a reflection of the intensification of the upper-level warm aloft, which acts as the primary driver of pressure falls in a rapidly intensifying tropical cyclone (*Zhang and Chen*, 2012).

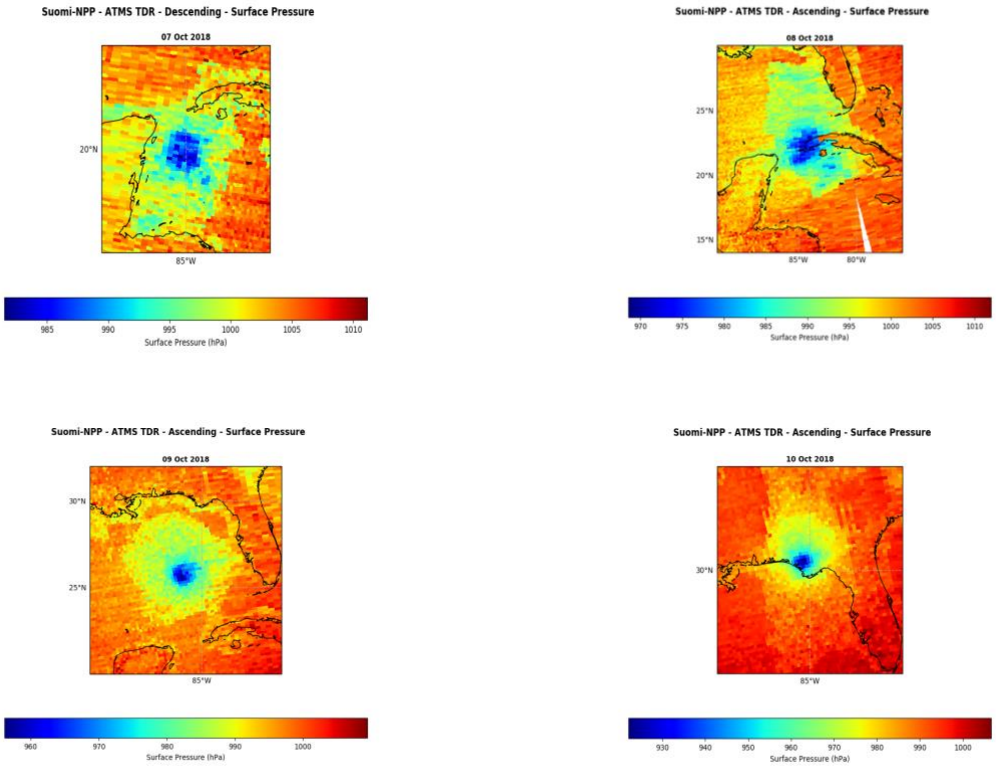

Figure 14*: Daily time series pressure plots of hurricane Michael derived from ATMS brightness temperature during 7 – 10 October 2018.*

However, one weakness of this surface pressure tendency calculation is its inability to resolve the changes in pressure when the tropical cyclone is located near the edge of the satellite scan. This is because existing errors and biases in the temperature retrieval algorithm are enhanced

at extreme beam positions. As a result, the script is unable to produce an intensification rate that matches the best track advisory data during that time. However, once the hurricane is no longer located at edge of the satellite scan, the algorithm is able to calculate a surface pressure tendency that once again matches well with best track pressure tendency. An example of this is shown in **Figure 9**, which presents a comparison of the calculated pressure tendency of Hurricane Dorian from ATMS data with surface pressure reported from advisory data. On September 1st, the center of the storm was located right on the edge of the satellite scan, which caused the temperature retrieval algorithm to introduce biases into the surface pressure calculation. The surface pressure tendency calculated was not large enough to match observations from the advisory data. As Hurricane Dorian moved away from the edge of the satellite scan on September 2nd, the temperature retrieval algorithm was once again able to accurately calculate atmospheric profiles, leading to improved calculations of surface pressure tendencies.

Another weakness of this study is that it uses temperature retrieval coefficients generated in a previous paper (*Yan et al.,* 2020), rather than calculating unique, storm-specific coefficients. This is a part of the future work for this project that will be incorporated into the temperature retrieval and surface pressure calculation. The next step will be calculating temperature retrieval coefficients for clear and cloudy sky conditions for each day during the duration of the hurricane of interest. Doing this should improve on the results found in this paper because the coefficients will correlate to ECMWF forecast analysis produced on the same day as the hurricane, rather than using coefficients calculated for similar, but not the exact same, atmospheric conditions.

Chapter 5 Summary and Conclusions

Sounding data collected by the ATMS instrument on board the Suomi-NPP and NOAA-20 satellites is valuable to observe the spatial and temporal evolution of tropical cyclones. One application of this data is to incorporate retrieved temperatures from the ATMS instrument with the hydrostatic equation to calculate surface pressure tendency. This algorithm would allow forecasters to observe changes to the surface pressure in a tropical cyclone in near real time based on the development of the upper-level warm core. ATMS channels 5 – 12 were used to convert brightness temperature to temperature in clear sky regions, while ATMS channels 7 – 12 were used in cloudy sky conditions (*Yan et al.,* 2020). This difference was required because of the contamination of microwave radiation caused by large raindrops in precipitation regions. As a result, the lower levels of the atmosphere where large drops are found would cause significant errors in temperature retrievals necessary for vertical temperature profiles (*Zhu et al.*, 2002; *Tian and Zou,* 2016; *Zhang et al.,* 2018; *Han et al.,* 2019).

The visualization software developed to display limb corrected ATMS brightness temperature allows users to analyze interesting meteorological phenomenon in the dataset, such as tropical cyclone development. Temperature retrievals allow vertical cross sections to be displayed through a hurricane, which show the development of the upper-level warm core as the storm develops, intensifies, weakens, and dissipates. This visualization software presents horizontal temperature fields at pressure levels from 100 to 1000 hPa to provide further context of the environment of the feature of interest, such as the warm core of a hurricane. It also calculates and plots surface pressure calculated from the temperatures retrieved from ATMS brightness temperature data. This allows users to analyze the accuracy of the pressure tendency being

calculated based on the characteristics of the warm core alone as compared to the best track advisory data pressure of an interesting tropical cyclone case.

The results of this study show that it is possible to track surface pressure tendency of tropical cyclones using temperature retrieved from ATMS brightness temperature with the hydrostatic equation. Surface pressure tendencies calculated for Hurricanes Dorian (2019), Florence (2018), and Michael (2018) all tracked reasonably well when compared with the best track advisory data. Future work would involve using the gradient wind balance equation to calculate wind speed tendencies of tropical cyclones, following *Kieu et al.* (2010), in combination with the surface pressure tendency methodology described in this study. These wind speeds would then be compared to the best track advisory data to determine how well this method could be applied to real-time applications for ongoing tropical cyclones. Also, improvements with handling temperature retrievals at the edge of the satellite scan and across coastlines would be beneficial in observing hurricane warm cores for storms in these locations. This would allow for a more robust surface pressure tendency calculation and would further enhance its value in handling real-time tropical cyclone events. Additionally, work will be done to incorporate unique temperature retrieval coefficients for each day during the lifecycle of a storm of interest. This should allow temperature retrievals to be better resolved, which will lead to more accurate surface pressure tendency results.

References

Beven II, J. L., R. Berg, and A. Hagen, 2019: Tropical cyclone report: Hurricane Michael (AL142018). 19 April 2019, 86 pp., https://www.nhc.noaa.gov/data/tcr/AL142018_Michael.pdf.

Carminati, F., S. Migliorinil, B. Ingleby, et al., 2019: Using reference radiosondes to characterise NWP model uncertainty for improved satellite calibration and validation. *Atmospheric Measurement Techniques*, **12**, 83–106, doi:10.5194/amt-12-83-2019

Durden, S. L., 2013: Observed Tropical Cyclone Eye Thermal Anomaly Profiles Extending above 300 hPa. *Monthly Weather Review*, **141**, 4256–4268, doi:10.1175/MWR-D-13-00021.1.

Goldberg, M. D., Crosby, David S., & Zhou, Lihang (2001). The limb adjustment of AMSU-A observations: Methodology and validation. *Journal of Applied Meteorology*, **40**, 70–83.

Goldberg, M. D., H. Kilcoyne, H. Cikanek, and A. Mehta, 2013: Joint Polar Satellite System: The United States next generation civilian polar-orbiting environmental satellite system, *J. Geophys. Res. Atmos.*, **118**(13) ,463–475, doi:10.1002/2013JD020389.

Han, Y., and F. Z. Weng, 2018: Remote sensing of tropical cyclone thermal structure from satellite microwave sounding instruments: Impacts of optimal channel selection on retrievals. *J. Meteor. Res.*, **32**(5), 804–818, doi:10.1007/s13351-018-8005-x.

Hu, H., F. Z. Weng, Y. Han, et al., 2019: Remote sensing of tropical cyclone thermal structure from satellite microwave sounding instruments: Impacts of background profiles on retrievals. *J. Meteor. Res.*, **33**(1), 89–103, doi:10.1007/s13351-019-8094-1.

Jordan, C. L., 1958: Mean Soundings for the West Indies Area. *J. Atmos. Sci.*, **15**, 91-97, doi:10.1175/1520-0469(1958)015<0091:MSFTWI>2.0.CO;2.

Kieu, C. Q., H. Chen, and D.-L. Zhang, 2010: An examination of the pressure - wind relationship in intense tropical cyclones. *Weather and Forecasting*, **25**, 895-907.

Spencer, R. W. and W. D. Braswell, 2001: Atlantic Tropical Cyclone Monitoring with AMSU-A: Estimation of Maximum Sustained Wind Speeds. *Monthly Weather Review*, **129**, 1518–1532, doi:10.1175/1520-0493(2001)129<1518:ATCMWA>2.0.CO;2.

Stern, D. P. and D. S. Nolan, 2012: On the height of the warm core in tropical cyclones. *Journal of the Atmospheric Sciences*, **69**(5), 1657–1680, doi:10.1175/JAS-D-11-010.1.

Stewart, S. R. and R. Berg, 2018: Tropical cyclone report: Hurricane Florence (AL062018). 3 May 2019, 98 pp., https://www.nhc.noaa.gov/data/tcr/AL062018_Florence.pdf.

Tian, X., and X. Zou, 2016: ATMS- and AMSU-A-derived hurricane warm core structures using a modified retrieval algorithm. *J. Geophys. Res. Atmos.*, **121**(12), 630–646, doi:10.1002/2016JD025042.

Weng F., X. Zou, N. Sun, et al., 2013: Calibration of Suomi national polar-orbiting partnership advanced technology microwave sounder. *J. Geophys. Res. Atmos.*, **118**, doi:10.1002/jgrd.50840

Yan, B., D. Liang, W. Porter, et al., 2020: Gap Filling of Advanced Technology Microwave Sounder Data as Applied to Hurricane Warm Core Animations. Submitted to *Earth and Space Science*.

Zhang, D.-L., and H. Chen, 2012: Importance of the upper-level warm core in the rapid intensification of a tropical cyclone. *Geophys. Res. Lett.*, **39**, L02806, doi:10.1029/2011GL050578.

Zhang, K., L. Zhou, M. Goldberg, X. Liu, W. Wolf, C. Tan, and Q. Liu, 2017: A methodology to adjust ATMS observations for limb effect and its applications. *Journal of Geophysical Research: Atmospheres*, **122**(11), 347–356, doi:10.1002/2017JD026820.

Zhu, T., D.-L. Zhang and F. Weng 2002: Impact of the Advanced Microwave Sounding Unit data on hurricane prediction. *Monthly Weather Review*, **130,** 2416-2432.

Zhu, T. and F. Weng, 2013: Hurricane Sandy warm-core structure observed from advanced Technology Microwave Sounder. *Geophysical Research Letters*, **40**, 3325-3330, doi:10.1002/grl.50626.

Zou, X. and X. Tian, 2018: Capturing Size and Intensity Changes of Hurricanes Irma and Maria (2017) from Polar-Orbiting Satellite Microwave Radiometers. *Journal of the Atmospheric Science*, **75**, doi:10.1175/JAS-D-17-0315.1.

Zou, X. and X. Tian, 2018: Hurricane warm-core retrievals from AMSU-A and remapped ATMS measurements with rain contamination eliminated. *Journal of Geophysical Research: Atmospheres*, **123**, doi:10.1029/2018JD028934.